

Semiconductor quantum-limited amplifier

D. Phan,¹ P. Falthansl-Scheinecker,¹ U. Mishra,¹ W.M. Strickland,² D. Langone,² J. Shabani,² and A.P. Higginbotham¹

¹*IST Austria, Am Campus 1, 3400 Klosterneuburg, Austria*

²*Department of Physics, New York University, New York, NY, 10003, USA*

(Dated: June 14, 2022)

Quantum-limited amplifiers are the first link in the quantum signal processing chain [1–3], allowing minute signals to be measured by noisy, classical electronics. Whereas later parts of the chain are dominated by semiconductor-based devices, the quantum-limited step can currently only be performed using metallic superconductors [4–12]. More broadly, the inherent scalability of semiconductors has motivated a great deal of research on quantum applications, including the scalable generation of quantum-control signals [13–15], and the processing of quantum information [16, 17] at fault-tolerant thresholds [18–22]. A semiconductor-based solution for the crucial task of quantum-limited amplification is, however, conspicuously absent. Here, we demonstrate a quantum-limited amplifier using a Josephson field-effect transistor (JoFET). The JoFET amplifier has 20 dB of gain with a 4 MHz instantaneous bandwidth, and a resonant frequency that is tunable over 2 GHz via the field effect. The gain is sufficient for integration into a measurement chain with conventional semiconductor amplifiers. Accordingly, we demonstrate a total added noise that approaches the fundamental limits placed by quantum mechanics. In contrast to metallic superconducting amplifiers, our device is compatible with magnetic fields. The JoFET amplifier completes the suite of semiconductor-based options for quantum control, information processing, and readout.

Aluminum-based tunnel junctions have proven to be more reliable and stable than any other platform, thanks to the formation of pristine Al-AlO_x interfaces through the natural oxidization of Al. Such a natural and coherent interface between a superconductor and a semiconductor has been missing until very recently. We use a wafer-scale method for the epitaxial growth of thin films of Al on InAs heterostructures (Al-InAs) [23–25] with atomically flat interfaces. Josephson junctions fabricated on these materials yield a voltage-controllable supercurrent with highly transparent contacts between Al and InAs quantum wells [26–28]. This epitaxial superconductor-semiconductor materials platform has recently been instrumental in exploring topological superconductivity [29–31], mesoscopic superconductivity [32] and voltage-tunable superconducting qubits [17]. Here

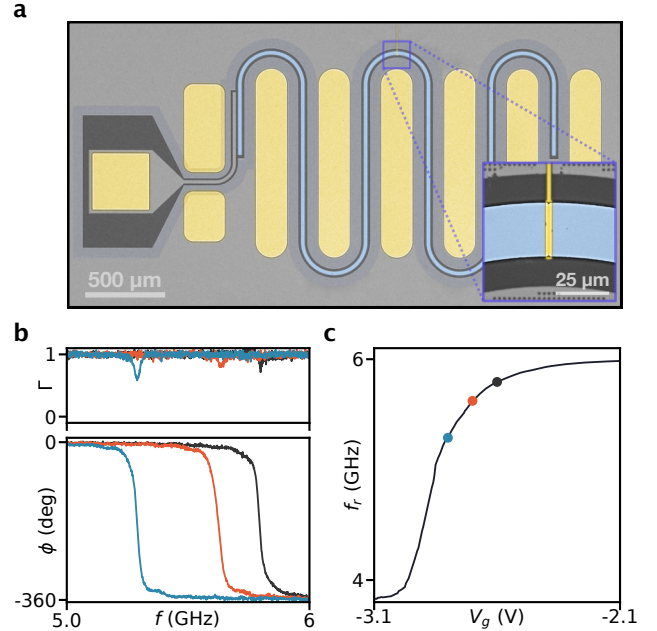


Figure 1. **Device and frequency modulation via the field effect.** **a**, False-colored image of the device (InP substrate dark gray, Nb light gray, aluminum light blue, Au yellow). A feed line (left) capacitively couples to the resonator, which is formed from an Al-InAs semiconductor heterostructure. Inset: Image of JoFET and electrostatic gate. **b**, Reflected signal magnitude Γ (top) and phase ϕ (bottom) versus signal frequency f at three different gate voltages V_g : -2.6 V (black), -2.7 V (orange), -2.8 V (blue), showing shift of resonance frequency with decreasing gate voltage. **c**, Resonant frequency f_r as a function of gate voltage V_g . Three dots with corresponding colors represent the three gate voltages in (b).

we introduce Al-InAs as the basis for quantum-limited signal processing devices.

The key operating element of our device is a Josephson field-effect transistor embedded in a microwave circuit (Fig. 1a). The microwave circuit is a half-wave coplanar waveguide microwave resonator coupled to a 50Ω transmission line, which forms the only measurement port. Ground planes of the device are formed from Nb with flux-pinning holes near the edges to improve magnetic-field resilience [33, 34]. The entire center pin of the resonator is made of Al/InAs, defined by chemical etch. The JoFET is also defined by selective removal of the Al, followed by atomic layer deposition of alumina, and finally

an electrostatic gate is defined with electron beam lithography and Au evaporation. Large Au chip-to-chip bond pads are also co-deposited in the final step to improve wire-bonding yield. The microwave reflection coefficient $R = \Gamma e^{i\phi}$ of a small incident signal is measured in a dilution refrigerator with a standard measurement chain, including a cryogenic commercial high-electron mobility transistor amplifier (HEMT).

The measured reflection coefficient displays a small dip in magnitude and a 360° winding of phase, signaling that the resonator is strongly coupled to the measurement port and that dissipation is weak (Fig. 1b). Fitting the reflection coefficient to a one-port model [35] gives a typical external coupling of $\kappa_{ex} = 30.6$ MHz, more than five times larger than the internal dissipation rate of $\kappa_{int} = 5.9$ MHz.

At gate voltages between saturation and pinch-off the JoFET contributes a tunable inductance to the microwave resonator, resulting in dramatic shifts in resonant frequency for small changes in gate voltage (Fig. 1b). The resonant frequency can be tuned over more than 2 GHz of bandwidth (Fig. 1c), exhibiting weak voltage dependence at extremal values, characteristic of a transistor reaching pinch-off and saturation. For resonant frequencies less than ~ 5 GHz we have observed a significant increase in microwave dissipation, presumably originating from the JoFET itself.

In addition to tunable inductance, the presence of the JoFET imparts a power-driven nonlinearity to the resonator [36]. Measuring the reflected phase as a function of signal frequency and power reveals that the resonant frequency smoothly decreases with increasing power (Fig. 2a). The output power from microwave sources is related to the resonator input power by an estimated total attenuation of 110 dB for all measurements. The downward shift in resonant frequency is accompanied by “sharpening” of the phase response (Fig. 2b). Downward shift in resonant frequency and an alteration in lineshape are key qualitative signatures of the required Kerr nonlinearity K for parametric amplification. Following Ref. [7], the nonlinearity can be estimated by referencing the input excitation power to an intracavity photon number. Measuring the downward frequency shift per photon as shown in Fig. 2c gives a typical value $K = -9.2$ kHz, which is suitable for parametric amplifiers [36]. The Kerr nonlinearity is tunable with gate voltage, going from negligible levels to several greater than 50 kHz in magnitude (Fig. 2d).

Parametric amplification is generated by applying a strong pump tone red detuned from the bare resonance frequency, in the vicinity of the phase “sharpening” features already identified close to the critical power Fig. 2b. Measuring scattering parameters with a weak probe signal reveals in excess of 20 dB of gain with a 4 MHz bandwidth, and a sharp phase response typical of a parametric amplifier (Fig. 3a,b). Modest detunings in the

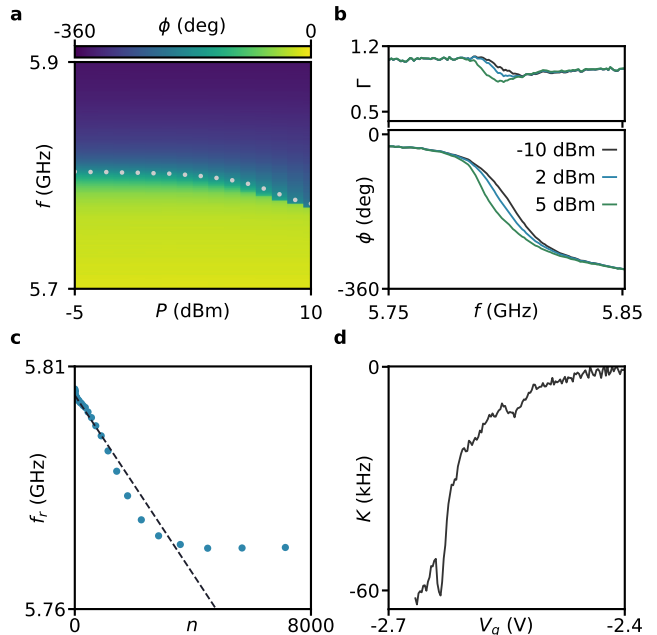


Figure 2. **Nonlinear response.** **a**, Reflected signal phase ϕ versus signal power P and frequency f . White dots indicate resonant frequencies f_r . **b**, Reflected magnitude Γ (top) and phase ϕ (bottom) versus f at different signal powers: low (black), medium (blue), and close to critical power (green). **c** Estimation of Kerr nonlinearity: resonant frequencies extracted from (a) versus average intracavity photon number n (dots). Slope of linear fit (dashed line) gives Kerr coefficient. **d** Gate-dependent Kerr coefficient (different dataset from c).

pump frequency do not substantially affect the amplifier response, but for large deviations the gain decreases to unity (Fig. 3b). Measuring the amplifier gain G as a function of pump frequency f_{pump} and power P_{pump} reveals a continuous region of maximum gain with an easily identifiable optimum operating region, as expected for a parametric amplifier (Fig. 3c). The power handling of the amplifier is quantified by measuring the gain for different signal powers. At very low input signal power where the average intracavity photon number is 0.01 (input power of -153 dBm, Fig. 3d), the gain saturates at 20.3 dB. Large input powers cause the amplifier gain to decrease, giving a 1 dB compression point of 2.9 intracavity photons (input power of -125 dBm) Fig. 3d. The gain, bandwidth, and compression point are comparable to values obtained with early, practically useful parametric amplifiers based on metallic Al/AIOx Josephson junctions [7, 8].

Quantum signals typically consist of few photons, making it crucial to achieve noise performance near the quantum limit. To assess the noise performance of the JoFET amplifier, a weak pilot signal is measured first with a commercial HEMT amplifier, and then with parametric gain activated (Fig. 4a). The JoFET amplifier dramatically improves the signal-to-noise ratio (SNR) of the

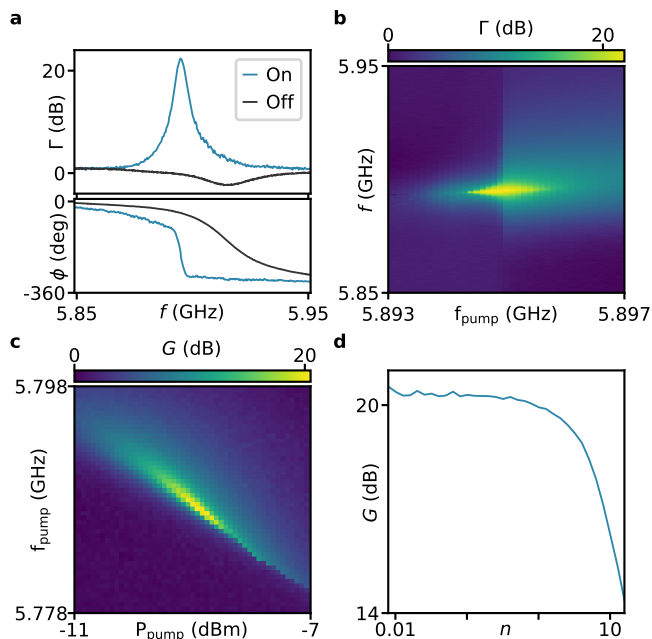


Figure 3. **Parametric gain.** **a**, Reflected signal magnitude Γ and phase ϕ measured as a function of signal frequency f from bare resonator (black) and pumped resonator (blue). **b**, Γ measured as a function of pump frequency f_{pump} and signal frequency f . The pump power is fixed slightly below the critical pump power at which the system bifurcates. $V_g = -2.5$ V for (a-b). **c**, Gain G inferred from the maximal reflected amplitude measured as a function of pump power P_{pump} and pump frequency f_{pump} , revealing line of maximum gain. $V_g = -2.55$ V. **d**, Gain G measured as a function of estimated average intracavity photon number n . $n = 0.01$ is approximately equivalent to $P_{\text{VNA}} = -43$ dBm and input power of -153 dBm. $V_g = -2.35$ V.

pilot-signal measurement. The total input-referred noise of the JoFET amplifier and subsequent measurement chain approaches the limits placed by quantum mechanics, which is $\frac{1}{2}$ of a photon from input vacuum fluctuations, and $\frac{1}{2}$ of a photon from nondegenerate amplification [2, 3], approximately equal to 0.285 K in temperature units. This noise measurement was carefully calibrated by varying the temperature of the mixing-chamber stage of the dilution refrigerator and measuring noise at various frequencies with the JoFET amplifier off (Fig. 4b). In the high temperature limit, the output noise is linear in temperature, with an offset that reflects the added noise of the HEMT, giving $T_{\text{HEMT}} = 1.63$ K at the JoFET operating frequency. At low temperature input-referred noise saturates. Calibrating over a wide range of frequencies reveals that noise saturation is pronounced only for high frequencies, confirming that that saturation is due to quantum, as opposed to thermal, fluctuations [3], and that these fluctuations are faithfully resolved by our calibration procedure.

Changing the pump frequency while keeping the sig-

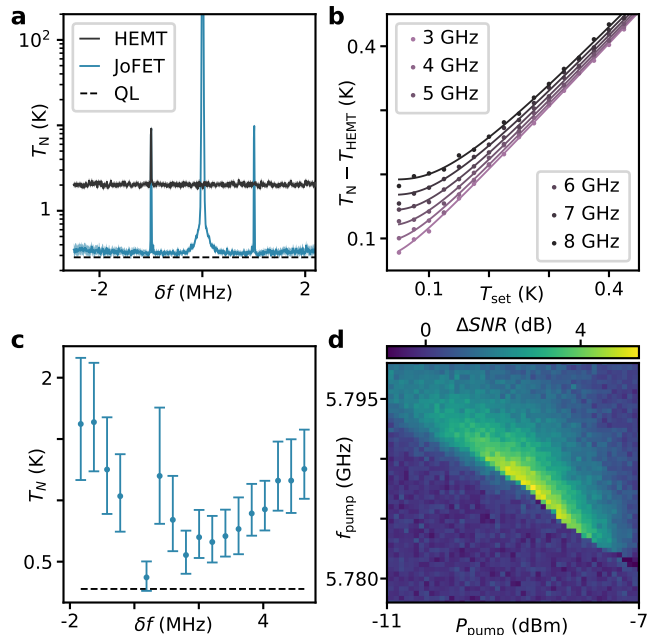


Figure 4. **Quantum-limited operation.** **a**, Total input-referred noise temperature T_N , measured in the presence of a weak pilot tone, as a function of detuning frequency from pump δf . Pump off (HEMT, black) and pump on (JoFET, blue) shown, in comparison with the quantum limit from input vacuum fluctuations and phase-preserving amplification (QL, dashed). Bands represent uncertainty propagated through from circuit parameters and HEMT noise calibration. $V_g = -2.35$ V. In JoFET data, the blue-detuned idler and the zero-detuned pump are also visible. **b**, Difference between total noise temperature T_N and HEMT added noise T_{HEMT} measured as a function of mixing chamber temperature setpoint T_{set} . Lines represent unity slope due to Johnson-Nyquist noise, corrected for the presence of vacuum fluctuations which dominate at low temperature and high frequency [3]. **c**, T_N measured as a function of pump-signal detuning δf by varying pump frequency with signal frequency fixed. One datapoint with a detuning of 2.7 kHz had to be removed from the dataset since the pump and signal could not be resolved individually. Error bars represent uncertainty propagated through from circuit parameters and HEMT noise calibration. **d**, Relative improvement in signal to noise ratio (ΔSNR) measured as a function of pump frequency f_{pump} and pump power P_{pump} : signal-pump detuning is fixed at 0.5 MHz, signal power is fixed at -43 dBm equivalent to 0.01 intracavity photon. $V_g = -2.55$ V for (c-d).

nal frequency fixed at 5.7839 GHz reveals that the noise performance is degraded if the pump frequency is away from the optimum operation region and if the detuning exceeds the amplifier bandwidth (Fig. 4c). By sweeping the pump frequency and the pump power with a fixed signal detuning, the optimum operating points of the amplifier can be extracted (Fig. 4d). The operating points with best noise performance corresponds to the regions of highest gain identified in Fig. 3c, as expected.

A technical advantage conferred by the Al-InAs hy-

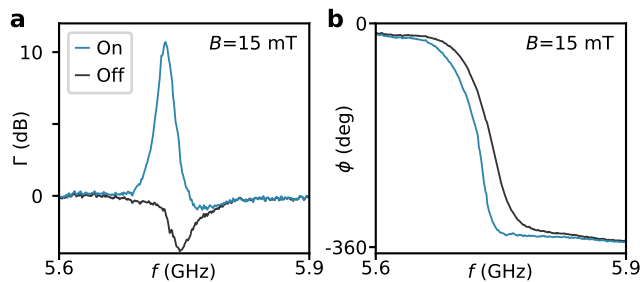


Figure 5. **Magnetic field compatibility.** Reflected magnitude Γ and (a), and phase ϕ (b) with and without pump tone as a function of probe frequency f in the presence of an in-plane magnetic field, $B = 15$ mT.

brid platform is compatibility with external fields. To explore the magnetic-field compatibility of the JoFET amplifier, we have steadily increased the parallel external magnetic field to 15 mT while compensating for small field misalignments with a perpendicular magnetic coil. Even with compensation, the resonator parameters evolve slightly in magnetic field, and a slight increase in loss is observed. Applying a pump tone gives an optimized gain of 10 dB (Fig. 5a-b). This demonstrates parametric amplification at a magnetic field order of magnitudes larger than the typical operating value for tunable metallic superconducting parametric amplifiers. Future experiments need to improve the resonator stability in magnetic field in order to allow a reliable noise measurement; we were unable to demonstrate quantum-limited operation in a magnetic field. Based on the high-field operation of gatemon qubits in similar material systems [37], a promising route to improving magnetic-field resilience of the JoFET amplifier would be to form the resonator center pin from a field-compatible superconductor that connects to a smaller Al/InAs microstructure.

Summarizing, we have demonstrated a quantum-limited and magnetic-field-compatible JoFET amplifier. Appealing future directions are to explore group IV materials, which could allow on-chip integration with spin qubit devices. It is also appealing to consider semiconductor solutions for other linear quantum signal processing devices such as modulators [38, 39] circulators [40, 41] or signal generators [42].

During preparation of this manuscript we became aware of related works demonstrating parametric amplification with graphene weak links [43, 44].

Acknowledgements We thank Shyam Shankar for helpful feedback on the manuscript. We gratefully acknowledge the support of the ISTA nanofabrication facility, MIBA machine shop and e-machine shop. NYU team acknowledges support from Army Research Office grant no. W911NF2110303.

Authorship contribution statement D. Phan performed nanofabrication. D. Phan, P. Falthansl-

Scheinecker, U. Mishra, and A.P. Higginbotham performed measurements. W.M. Strickland, D. Langone, and J. Shabani grew the Al/InAs heterostructure. D. Phan, A.P. Higginbotham, and J. Shabani designed the experiment. D. Phan, P. Falthansl-Scheinecker, U. Mishra, W.M. Strickland, and J. Shabani prepared the work for publication.

Data availability Raw data for all plots in the main text and supplement will be included with the manuscript before publication. Further data available upon reasonable request.

Methods

Sample preparation. The JoFET amplifier was fabricated from Al-proximitized InAs quantum well which was grown on a semi-insulating, Fe counter-doped (100) InP wafer. All the patterns were transferred with Raith EBPG 5100 electron beam lithography system. The Josephson weak link was made by etching a trench in the aluminum layer in the commercial etchant Transene D at 50 degrees C for 5 seconds. The trench was designed to be 20 nm long and 25 μ m wide. SEM imaging later showed that the trench width was about 50nm. The superconductor-semiconductor mesa forming the center pin of the CPW resonator was formed by masking with PMMA followed by a semiconductor wet etch in a mixture of $\text{CH}_3\text{COOH} : \text{H}_2\text{O}_2 : \text{H}_3\text{PO}_4$ for 150 seconds at room temperature. The ground plane was constructed by evaporating Ti 5nm, Nb 50nm following a short 1-min Ar ion milling at an accelerating voltage of 400V, with an ion current of 21mA in a Plassys UHV evaporator. In the next step, the dielectric layer separating the gate and the junction was deposited with an Oxford ALD system running a thermal ALD alumina process at 150 degrees C in 150 cycles, which gave an approximated thickness of 12nm. Eventually, the gate that covers just the area of the Josephson weak link was created by evaporating Ti 8nm and Au 80nm at a tilt angle of 30 degrees with 5 RPM planetary rotation in a Plassys HV evaporator. Due to low adhesion of Al bond wire to Nb ground plane, co-deposited Au bond pads are used to enhance Al alloy formation during wire bonding, hence, chip-to-chip bond yield. All lift-off and cleaning processes were performed in hot acetone at 50 degrees C and isopropanol.

Measurements. The sample was mounted on a copper bracket on a home made printed circuit board. We used a vector network analyzer (VNA) model Keysight P9372A to measure R . A Rohde & Schwarz signal generator model SGS100A was used to provide the pump tone. When pumping at a fixed frequency, we used the VNA to provide a small probe signal and measure the gain profile from the reflected monotone at probe frequency. A home-made IVVI voltage source provided the gate bias. To achieve gain, we typically set the gate voltage to -2.5 V and swept the VNA power until the response became critical. Consequentially, a pump tone from the R&S signal generator was injected at a power of about 1 dB

below the approximated critical power and slightly above the critical frequency. The probe power from the VNA was reduced to maintain the validity of the stiff pump condition. We tuned up the JoFET amplifier by sweeping the pump frequency and power in the proximity of the nonlinear resonator's critical values and recording the maximal reflected amplitude at the VNA input. Optimal amplification configurations were then found by fine sweeping around the regions where the maximal gains were highest, whose values were typically more than 20 dB. To measure the noise, we recorded the power spectral density from the output of the JoFET amplifier by a ThinkRF R5550 hybrid spectrum analyzer. In-plane magnetic field and compensation was applied by a vector magnet system of the Oxford Triton fridge and Mercury iPS power supply.

Kerr nonlinearity extraction from power sweep. The dependence of resonance frequency on input power was used to estimate the Kerr nonlinearity K similar to [7]. Resonant frequency decreased linearly with increasing average intracavity photon number following the Hamiltonian [36]:

$$H_{\text{JPA}} = \hbar \left(\tilde{\omega}_0 + \frac{K}{2} \langle A^\dagger A \rangle \right) A^\dagger A. \quad (1)$$

In the above Hamiltonian, the intracavity field was assumed to be coherent. We fit the expression for the resonant frequency inside the parentheses to the frequency of the dips in the reflections in Fig 2ab in the non-bifurcated regime to extract K .

JoFET amplifier design. CPW resonator was designed to have a characteristic impedance of 50 Ω with the center conductor with and gap of 25 μm and 16 μm . Resonator length was chosen so that the resonant frequency of 6 GHz at base temperature. To account for the kinetic inductance of the 10 nm-thick Al layer, geometric resonant frequency was designed to be 7.2 GHz so that result resonance would drop to 6 GHz based on previous fabrication experience. The kinetic inductance of the Al film fluctuates from device to device, presumably due to uncontrolled oxidation of the Al. The JoFET was designed for a maximal critical current of 10 μmA which gives a zeroth order Kerr nonlinearity K of 1.4 kHz at zero bias and in this CPW configuration, such that the device can be gated into a regime appropriate for amplification [36]. Designed dimensions were chosen based on our previous lithography tests and critical current measurements where a sheet critical current density of 0.38 $\mu\text{A}/\mu\text{m}$ was achieved.

JoFET input noise referral. Noise referred to the input of the HEMT was measured as described in Fig. 4b. To refer noise to the input of the JoFET amplifier, we determine the JoFET amplifier frequency response from a Lorentzian fit to the measured noise spectrum, and determine the overall gain level from the pilot signals, accounting for their nonzero detuning. Noise is input-referred by

dividing by the full JoFET gain profile, accounting for the nonzero loss in the microwave circuit.

-
- [1] H. A. Haus and J. A. Mullen, "Quantum noise in linear amplifiers," *Phys. Rev.* **128**, 2407–2413 (1962).
 - [2] Carlton M. Caves, "Quantum limits on noise in linear amplifiers," *Phys. Rev. D* **26**, 1817–1839 (1982).
 - [3] A. A. Clerk, M. H. Devoret, S. M. Girvin, Florian Marquardt, and R. J. Schoelkopf, "Introduction to quantum noise, measurement, and amplification," *Rev. Mod. Phys.* **82**, 1155–1208 (2010).
 - [4] B. Yurke, L. R. Corruccini, P. G. Kaminsky, L. W. Rupp, A. D. Smith, A. H. Silver, R. W. Simon, and E. A. Whittaker, "Observation of parametric amplification and deamplification in a josephson parametric amplifier," *Phys. Rev. A* **39**, 2519–2533 (1989).
 - [5] R. Movshovich, B. Yurke, P. G. Kaminsky, A. D. Smith, A. H. Silver, R. W. Simon, and M. V. Schneider, "Observation of zero-point noise squeezing via a josephson-parametric amplifier," *Phys. Rev. Lett.* **65**, 1419–1422 (1990).
 - [6] B. Yurke, M. L. Roukes, R. Movshovich, and A. N. Pargellis, "A low-noise series-array josephson junction parametric amplifier," *Applied Physics Letters* **69**, 3078–3080 (1996), <https://doi.org/10.1063/1.116845>.
 - [7] M. A. Castellanos-Beltran and K. W. Lehnert, "Widely tunable parametric amplifier based on a superconducting quantum interference device array resonator," *Applied Physics Letters* **91**, 083509 (2007), <https://doi.org/10.1063/1.2773988>.
 - [8] M. A. Castellanos-Beltran, K. D. Irwin, G. C. Hilton, L. R. Vale, and K. W. Lehnert, "Amplification and squeezing of quantum noise with a tunable josephson metamaterial," *Nature Physics* **4**, 929–931 (2008).
 - [9] N. Bergeal, F. Schackert, M. Metcalfe, R. Vijay, V. E. Manucharyan, L. Frunzio, D. E. Prober, R. J. Schoelkopf, S. M. Girvin, and M. H. Devoret, "Phase-preserving amplification near the quantum limit with a josephson ring modulator," *Nature* **465**, 64–68 (2010).
 - [10] C. Macklin, K. O'Brien, D. Hover, M. E. Schwartz, V. Bolkhovskiy, X. Zhang, W. D. Oliver, and I. Siddiqi, "A near-quantum-limited josephson traveling-wave parametric amplifier," *Science* **350**, 307–310 (2015), <https://www.science.org/doi/pdf/10.1126/science.aaa8525>.
 - [11] Luca Planat, Arpit Ranadive, Rémy Dassonneville, Javier Puertas Martínez, Sébastien Léger, Cécile Naud, Olivier Buisson, Wiebke Hasch-Guichard, Denis M. Basko, and Nicolas Roch, "Photonic-crystal josephson traveling-wave parametric amplifier," *Phys. Rev. X* **10**, 021021 (2020).
 - [12] N. E. Frattini, V. V. Sivak, A. Lingenfelter, S. Shankar, and M. H. Devoret, "Optimizing the nonlinearity and dissipation of a snail parametric amplifier for dynamic range," *Phys. Rev. Applied* **10**, 054020 (2018).
 - [13] S. J. Pauka, K. Das, R. Kalra, A. Moini, Y. Yang, M. Trainer, A. Bousquet, C. Cantaloube, N. Dick, G. C. Gardner, M. J. Manfra, and D. J. Reilly, "A cryogenic cmos chip for generating control signals for multiple qubits," *Nature Electronics* **4**, 64–70 (2021).
 - [14] Xiao Xue, Bishnu Patra, Jeroen P. G. van Dijk, Nodar

- Samkharadze, Sushil Subramanian, Andrea Corna, Brian Paquelet Wuetz, Charles Jeon, Farhana Sheikh, Esdras Juarez-Hernandez, Brando Perez Esparza, Huzaifa Ramapurawala, Brent Carlton, Surej Ravikumar, Carlos Nieva, Sungwon Kim, Hyung-Jin Lee, Amir Sammak, Giordano Scappucci, Menno Veldhorst, Fabio Sebastiano, Masoud Babaie, Stefano Pellerano, Edoardo Charbon, and Lieven M. K. Vandersypen, “Cmos-based cryogenic control of silicon quantum circuits,” *Nature* **593**, 205–210 (2021).
- [15] F. Lecocq, F. Quinlan, K. Cicak, J. Aumentado, S. A. Diddams, and J. D. Teufel, “Control and readout of a superconducting qubit using a photonic link,” *Nature* **591**, 575–579 (2021).
- [16] T. W. Larsen, K. D. Petersson, F. Kuemmeth, T. S. Jespersen, P. Krogstrup, J. Nygård, and C. M. Marcus, “Semiconductor-nanowire-based superconducting qubit,” *Phys. Rev. Lett.* **115**, 127001 (2015).
- [17] Lucas Casparis, Malcolm R. Connolly, Morten Kjaergaard, Natalie J. Pearson, Anders Kringhøj, Thorvald W. Larsen, Ferdinand Kuemmeth, Tiantian Wang, Candice Thomas, Sergei Gronin, Geoffrey C. Gardner, Michael J. Manfra, Charles M. Marcus, and Karl D. Petersson, “Superconducting gatemon qubit based on a proximitized two-dimensional electron gas,” *Nature Nanotechnology* **13**, 915–919 (2018).
- [18] M. Veldhorst, J. C. C. Hwang, C. H. Yang, A. W. Leenstra, B. de Ronde, J. P. Dehollain, J. T. Muhonen, F. E. Hudson, K. M. Itoh, A. Morello, and A. S. Dzurak, “An addressable quantum dot qubit with fault-tolerant control-fidelity,” *Nature Nanotechnology* **9**, 981–985 (2014).
- [19] Kenta Takeda, Jun Kamioka, Tomohiro Otsuka, Jun Yoneda, Takashi Nakajima, Matthieu R. Delbecq, Shinichi Amaha, Giles Allison, Tetsuo Kodera, Shunri Oda, and Seigo Tarucha, “A fault-tolerant addressable spin qubit in a natural silicon quantum dot,” *Science Advances* **2**, e1600694 (2016), <https://www.science.org/doi/pdf/10.1126/sciadv.1600694>.
- [20] Jun Yoneda, Kenta Takeda, Tomohiro Otsuka, Takashi Nakajima, Matthieu R. Delbecq, Giles Allison, Takumu Honda, Tetsuo Kodera, Shunri Oda, Yusuke Hoshi, Noritaka Usami, Kohei M. Itoh, and Seigo Tarucha, “A quantum-dot spin qubit with coherence limited by charge noise and fidelity higher than 99.9%,” *Nature Nanotechnology* **13**, 102–106 (2018).
- [21] Akito Noiri, Kenta Takeda, Takashi Nakajima, Takashi Kobayashi, Amir Sammak, Giordano Scappucci, and Seigo Tarucha, “Fast universal quantum gate above the fault-tolerance threshold in silicon,” *Nature* **601**, 338–342 (2022).
- [22] Xiao Xue, Maximilian Russ, Nodar Samkharadze, Brennan Undseth, Amir Sammak, Giordano Scappucci, and Lieven M. K. Vandersypen, “Computing with spin qubits at the surface code error threshold,” arXiv:2107.00628 (2022).
- [23] J. Shabani, M. Kjaergaard, H. J. Suominen, Younghyun Kim, F. Nichele, K. Pakrouski, T. Stankevic, R. M. Lutchyn, P. Krogstrup, R. Feidenhans’l, S. Kraemer, C. Nayak, M. Troyer, C. M. Marcus, and C. J. Palmstrøm, “Two-dimensional epitaxial superconductor-semiconductor heterostructures: A platform for topological superconducting networks,” *Phys. Rev. B* **93**, 155402 (2016).
- [24] Wendy L. Sarney, Stefan P. Svensson, Kaushini S. Wickramasinghe, Joseph Yuan, and Javad Shabani, “Reactivity studies and structural properties of al on compound semiconductor surfaces,” *Journal of Vacuum Science & Technology B* **36**, 062903 (2018), <https://doi.org/10.1116/1.5053987>.
- [25] Wendy L. Sarney, Stefan P. Svensson, Asher C. Leff, William F. Schiela, Joseph O. Yuan, Matthieu C. Dartiailh, William Mayer, Kaushini S. Wickramasinghe, and Javad Shabani, “Aluminum metallization of iii–v semiconductors for the study of proximity superconductivity,” *Journal of Vacuum Science & Technology B* **38**, 032212 (2020), <https://doi.org/10.1116/1.5145073>.
- [26] M. Kjaergaard, F. Nichele, H. J. Suominen, M. P. Nowak, M. Wimmer, A. R. Akhmerov, J. A. Folk, K. Flensberg, J. Shabani, C. J. Palmstrøm, and C. M. Marcus, “Quantized conductance doubling and hard gap in a two-dimensional semiconductor–superconductor heterostructure,” *Nature Communications* **7**, 12841 (2016).
- [27] William Mayer, Joseph Yuan, Kaushini S. Wickramasinghe, Tri Nguyen, Matthieu C. Dartiailh, and Javad Shabani, “Superconducting proximity effect in epitaxial al–inas heterostructures,” *Applied Physics Letters* **114**, 103104 (2019).
- [28] Matthieu C. Dartiailh, Joseph J. Cuozzo, Bassel H. Elfeky, William Mayer, Joseph Yuan, Kaushini S. Wickramasinghe, Enrico Rossi, and Javad Shabani, “Missing shapiro steps in topologically trivial josephson junction on InAs quantum well,” *Nature Communications* **12**, 78 (2021).
- [29] Fabrizio Nichele, Asbjørn C. C. Drachmann, Alexander M. Whiticar, Eoin C. T. O’Farrell, Henri J. Suominen, Antonio Fornieri, Tian Wang, Geoffrey C. Gardner, Candice Thomas, Anthony T. Hatke, Peter Krogstrup, Michael J. Manfra, Karsten Flensberg, and Charles M. Marcus, “Scaling of majorana zero-bias conductance peaks,” *Phys. Rev. Lett.* **119**, 136803 (2017).
- [30] Antonio Fornieri, Alexander M. Whiticar, F. Setiawan, Elías Portolés, Asbjørn C. C. Drachmann, Anna Keselman, Sergei Gronin, Candice Thomas, Tian Wang, Ray Kallahaer, Geoffrey C. Gardner, Erez Berg, Michael J. Manfra, Ady Stern, Charles M. Marcus, and Fabrizio Nichele, “Evidence of topological superconductivity in planar josephson junctions,” *Nature* **569**, 89–92 (2019).
- [31] Matthieu C. Dartiailh, William Mayer, Joseph Yuan, Kaushini S. Wickramasinghe, Alex Matos-Abiague, Igor Žutić, and Javad Shabani, “Phase signature of topological transition in josephson junctions,” *Phys. Rev. Lett.* **126**, 036802 (2021).
- [32] C. G. L. Bøttcher, F. Nichele, M. Kjaergaard, H. J. Suominen, J. Shabani, C. J. Palmstrøm, and C. M. Marcus, “Superconducting, insulating and anomalous metallic regimes in a gated two-dimensional semiconductor–superconductor array,” *Nature Physics* **14**, 1138–1144 (2018).
- [33] N. Samkharadze, A. Bruno, P. Scarlino, G. Zheng, D. P. DiVincenzo, L. DiCarlo, and L. M. K. Vandersypen, “High-kinetic-inductance superconducting nanowire resonators for circuit qed in a magnetic field,” *Phys. Rev. Applied* **5**, 044004 (2016).
- [34] J.G. Kroll, F. Borsoi, K.L. van der Enden, W. Uilhoorn, D. de Jong, M. Quintero-Pérez, D.J. van Woerkom, A. Bruno, S.R. Plissard, D. Car, E.P.A.M. Bakkers, M.C. Cassidy, and L.P. Kouwenhoven, “Magnetic-

- field-resilient superconducting coplanar-waveguide resonators for hybrid circuit quantum electrodynamics experiments,” *Phys. Rev. Applied* **11**, 064053 (2019).
- [35] D. F. Walls and G. J. Milburn, *Quantum Optics* (Springer Berlin, Heidelberg, 1994).
- [36] Christopher Eichler and Andreas Wallraff, “Controlling the dynamic range of a josephson parametric amplifier,” *EPJ Quantum Technology* **1**, 2 (2014).
- [37] A. Kringhøj, T. W. Larsen, O. Erlandsson, W. Uilhoorn, J.G. Kroll, M. Hesselberg, R.P.G. McNeil, P. Krogstrup, L. Casparis, C.M. Marcus, and K.D. Petersson, “Magnetic-field-compatible superconducting transmon qubit,” *Phys. Rev. Applied* **15**, 054001 (2021).
- [38] N. Bergeal, R. Vijay, V. E. Manucharyan, I. Siddiqi, R. J. Schoelkopf, S. M. Girvin, and M. H. Devoret, “Analog information processing at the quantum limit with a josephson ring modulator,” *Nature Physics* **6**, 296–302 (2010).
- [39] Benjamin J. Chapman, Eric I. Rosenthal, Joseph Kerckhoff, Leila R. Vale, Gene C. Hilton, and K. W. Lehnert, “Single-sideband modulator for frequency domain multiplexing of superconducting qubit readout,” *Applied Physics Letters* **110**, 162601 (2017), <https://doi.org/10.1063/1.4981390>.
- [40] Benjamin J. Chapman, Eric I. Rosenthal, Joseph Kerckhoff, Bradley A. Moores, Leila R. Vale, J. A. B. Mates, Gene C. Hilton, Kevin Lalumière, Alexandre Blais, and K. W. Lehnert, “Widely tunable on-chip microwave circulator for superconducting quantum circuits,” *Phys. Rev. X* **7**, 041043 (2017).
- [41] Benjamin J. Chapman, Eric I. Rosenthal, and K. W. Lehnert, “Design of an on-chip superconducting microwave circulator with octave bandwidth,” *Phys. Rev. Applied* **11**, 044048 (2019).
- [42] M. C. Cassidy, A. Bruno, S. Rubbert, M. Irfan, J. Kammhuber, R. N. Schouten, A. R. Akhmerov, and L. P. Kouwenhoven, “Demonstration of an ac josephson junction laser,” *Science* **355**, 939–942 (2017), <https://www.science.org/doi/pdf/10.1126/science.aah6640>.
- [43] Guillaume Butseraen, Arpit Ranadive, Nicolas Aparicio, Kazi Rafsanjani Amin, Abhishek Juyal, Martina Esposito, Kenji Watanabe, Takashi Taniguchi, Nicolas Roch, François Lefloch, and Julien Renard, “A gate-tunable graphene josephson parametric amplifier,” arXiv:2204.02175 (2022).
- [44] Joydip Sarkar, Kishor V. Salunkhe, Supriya Mandal, Subhamoy Ghatak, Alisha H. Marchawala, Ipsita Das, Kenji Watanabe, Takashi Taniguchi, R. Vijay, and Mandar M. Deshmukh, “Quantum noise limited microwave amplification using a graphene josephson junction,” arXiv:2204.02103 (2022), 10.48550/ARXIV.2204.02103.